Hindawi
Mathematical Problems in Engineering
Volume 2017, Article ID 7834621, 11 pages
https://doi.org/10.1155/2017/7834621

Research Article

Bending Angle Prediction Model Based on BPNN-Spline in Air Bending Springback Process

Zhefeng Guo and Wencheng Tang

Department of Mechanical Engineering, Southeast University, Nanjing 211189, China

Correspondence should be addressed to Wencheng Tang; tangwc@seu.edu.cn

Received 16 October 2016; Revised 16 January 2017; Accepted 7 February 2017; Published 27 February 2017

Academic Editor: Marek Lefik

In order to rapidly and accurately predict the springback bending angle in V-die air bending process, a springback bending angle prediction model on the combination of error back propagation neural network and spline function (BPNN-Spline) is presented in this study. An orthogonal experimental sample set for training BPNN-Spline is obtained by finite element simulation. Through the analysis of network structure, the BPNN-Spline black box function of bending angle prediction is established, and the advantage of BPNN-Spline is discussed in comparison with traditional BPNN. The results show a close agreement with simulated and experimental results by application examples, which means that the BPNN-Spline model in this study has higher prediction accuracy and better applicable ability. Therefore, it could be adopted in a numerical control bending machine system.

1. Introduction

The sheet metal bending is an essential metalworking process in many industries [1], wherein V-die air bending is a main topic in the stamping field. The flat sheet is bent to a curved sheet by the pressing on the bending machine. Because of the existence of elastic deformation in curved sheet, springback will occur during the unloaded process of curved sheet in the bending machine. As a result, the final bending angle of curved sheet will be obtained.

Mohammadi et al. [2] have developed a springback prediction analytical formulation for sandwich sheets based on a wrap-around assumption and primary bending theories. Numerical simulation and experiments have been carried out to verify the effect of punch radius, die opening, and punch stroke on springback. Results showed that the springback is increased with an increase in punch stroke, punch radius, and die opening. De Vin [3] has presented an air bending geometric model. This model has been found to be convenient to calculate the bending angle.

Finite element (FE) simulation is a popular method at present [4], due to low time costs and simple operation. Vorkov et al. [5] have studied the springback of different types of high-strength steels using FE model. The material properties and a correct material model for high-strength steels have been obtained and built, respectively. Fu et al. [6] have developed a material constitutive model based on Hill's yielding criterion under plane strain conditions. The multiple step incremental air bending forming and springback processes have been simulated. Jamli et al. [7] have developed an artificial neural network based on constitutive model which can be used in the FE code through user defined material subroutine. FE analysis procedures have been carried out for the springback prediction of sheet metal based on an L-bending experiment. The FE analysis presented an improvement in the prediction accuracy in comparison with the measured data.

The approximate model can be chosen to replace the FE simulation. When the approximate model is established, the response of research parameters is obtained immediately. Approximate model is an efficient research method to reduce the time consumption. Many kinds of approximate model are able to achieve the approximation of bending springback process, such as artificial neural network [8–11], radial basis function [12, 13], and response surface method [14, 15]. The error backpropagation neural network (BPNN) is one of

the widely used and successful networks at present. It is particularly useful in process modeling and has been used in diverse applications, such as control, robotics, pattern recognition, forecasting, and manufacturing optimization [16]. In general, the approximate model needs a lot of samples. Orthogonal experiment [17–19], Latin hypercube design [20], and so forth can reduce the number of samples under the same approximate calculation accuracy.

FE simulation and theory calculation method are mainly used to research the V-die air bending springback process at present. Theory calculation method has better general property and faster prediction speed. However, there are many inevitable assumptions in calculation model which will result in low calculation accuracy. In terms of the FE simulation, at least to the authors' knowledge, one FE model only simulates one group of bending data. Although it generates more accurate result, it is not speedy enough for bending angle prediction. In addition, the technical requirement for the user on FE software is higher. Therefore, there is a need towards an accurate, general, speedier, and more maneuverable means to predict the bending angle.

In this study, the authors propose a springback bending angle prediction model which is the combination of BPNN and spline function (BPNN-Spline). The BPNN-Spline combined model is expressed by simple mathematical formulas. The complex numerical simulation process will be turned into a simple mathematical calculation procedure. It enables a faster and maneuverable bending angle prediction in comparison with FE simulation. Besides, the BPNN-Spline combined model is developed by the accurate FE simulation results, where the prediction accuracy is relatively high. It will offset the disadvantages of FE simulation and theory calculation method at the same time. Due to the full utilization of better generalization ability of BPNN and smooth feature of the spline function, the model outperforms traditional BPNN model. Also, through the test of application examples, the general and precise properties of BPNN-Spline are also fully demonstrated. During the bending process, input the parameters to the BPNN-Spline black box; the springback bending angle is obtained immediately. Consequently, as a computation method, the model can be applied properly in a bending machine numerical control system.

2. Introduction of Air Bending Springback Process

The flat metal sheet is bent into a curved sheet with angle α_0 on the bending machine, as shown in Figure 1(a). Due to the existence of material elasticity, when the punch is unloaded, the springback will occur, and the curved sheet will become angle α (hereinafter uniformly referred to as bending angle) from α_0, as shown in Figure 1(b), where V, R, r, t, φ, and D are the nominal width of die notch, die corner radius, punch corner radius, sheet thickness, die angle, and punch displacement, respectively.

Bending angle α is related to various process parameters, such as material, sheet thickness, and tool corner radius. When other process parameters are determined, the value of α will correspond to the value of D. The desired α can be obtained by reasonable adjustment of D. The purpose of this study is to develop a bending angle prediction model which is suitable for bending machine numerical control system. This model provides a precise mapping relation between D and α under diverse process parameters.

Table 1: Parameters of research materials.

Material	E (GPa)	K (MPa)	n	σ_s (MPa)	M
DC06	207	530	0.24	126	0.61
SUS304	207	1455	0.5	239	1.15
DP600	207	1099	0.179	382	1.85
B340LA	207	678	0.16	400	1.93
6111-T4	69	549	0.235	143	2.07

3. FE Simulation of Bending Springback Process

3.1. Research Materials and Parameter Levels. The bending angle is closely related to the material plasticity. In general, the relation between stress and strain of material plasticity could be obtained from tensile test. Then, through a series of transformation and fitting, the exponential form relation curve between true stress and true strain can be considered as follows:

$$\begin{aligned} \sigma &= E\varepsilon, \quad (\varepsilon \le \varepsilon_0) \\ \sigma &= K\varepsilon^n, \quad (\varepsilon > \varepsilon_0), \end{aligned} \tag{1}$$

where K, n, and ε_0 are the hardening coefficient, hardening exponent, and yield strain, respectively.

In this study, material parameters are determined based on tensile tests, as listed in Table 1. For the tensile test of one material, the material parameters of different sheet thickness are lightly different. The error caused by different sheet thickness is a micro amount with respect to the error caused by approximate prediction system. Therefore, in order to facilitate the operation, the variation of material parameter with different sheet thickness is not considered.

As for the BPNN, the factor property should be measurable. One material has many measurable parameters such as K, n, and ε_0 at the same time. Each material is indicated by an integrated value $1000 * \sigma_s/E(M)$, as listed in Table 1, where E and σ_s are Young's modulus and yield stress, respectively.

In this study, to develop the springback bending angle prediction model, t, R, r, M, and D are the input parameters, and bending angle α is the output. The various parameters are listed in Table 2. V and φ are 12 mm and 86°, respectively.

3.2. Orthogonal Experimental Design. To further reduce the number of simulations, the orthogonal experimental design is implemented in this study. Orthogonal experimental design is an efficient design method whose features are uniform distribution and comparable order. The orthogonal experimental design sample sets are listed in Table 3.

The outputs of Table 3 are the bending angles α_1~α_5 which are obtained through FE simulation. The measurement

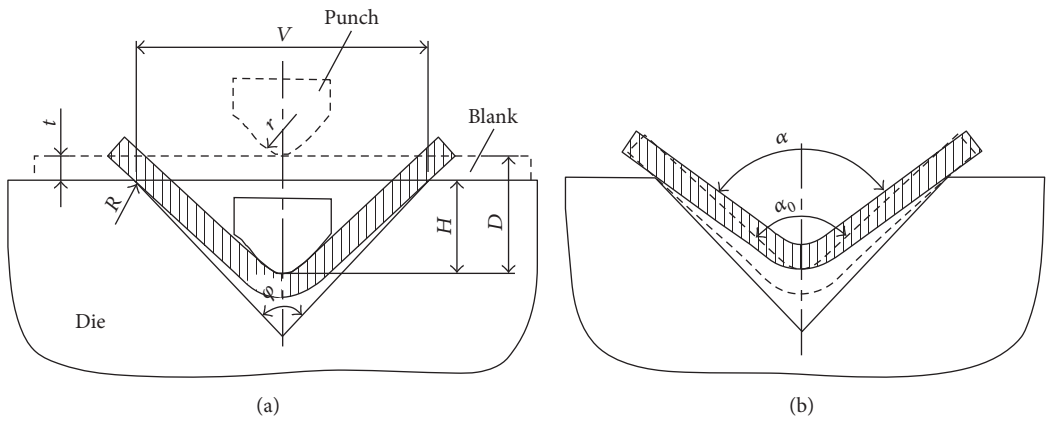

Figure 1: Sheet bending springback process diagram: (a) curved sheet before springback; (b) curved sheet after springback.

Table 2: Variable parameters with their levels.

Level	t (mm)	R (mm)	r (mm)	M	D (mm)
1	1	0.2	0.2	0.61	5
2	1.4	0.6	0.6	1.15	4.4
3	2	1	1	1.85	4
4	—	—	—	1.93	3
5	—	—	—	2.07	2.6

unit of α_i is degree. Each α_i corresponds to certain punch displacement D_i in FE simulation. D_i are 5 mm, 4.4 mm, 4 mm, 3 mm, and 2.6 mm, respectively. The anterior 25 samples in Table 3 are the orthogonal experiment sample sets for training the BPNN, and the extra 5 samples are selected randomly from full factorial design to test the accuracy of BPNN.

Table 3 shows that the bending angles on the same D_i are different for different materials and bending process parameters. But the bending angles on the same D_i are more close to each other in comparison with those bending angles of different D_i. The factor D_i is more important for the value of bending angle.

3.3. FE Model of Bending Springback Process. FE software ABAQUS is used to simulate the bending springback process. In the bending and springback process, sheet sectional deformation of width direction is almost the same. 2D elements have been used in the FE model in order to reduce the simulation time. In the FE, the surface to surface contact model is adopted where the coulomb friction law is considered. The friction coefficient is set to 0.1 as an ordinary scale of metal contact. The punch and die are considered as rigid body. Element type is chosen as the four-node bilinear plane stress quadrilateral element (CPS4R). The mesh division figure is shown in Figure 2. The remaining parameters are set to the default of the software.

As it is shown in Table 3, some bending angles are even less than the die angle φ which is equal to 86°. Since some materials in Table 1 have bigger hardening exponent value such as SUS304, these materials affect the material strengthening in bending process. The curved sheet arcs of these materials are large. If D is larger, the large curved sheet arc will be bent for the second time when the low surface touches the inner wall of die notch, as shown in Figure 3. It is inevitable that the bending angle is less than die angle. However, the sheet only touches the die corner radius for most material.

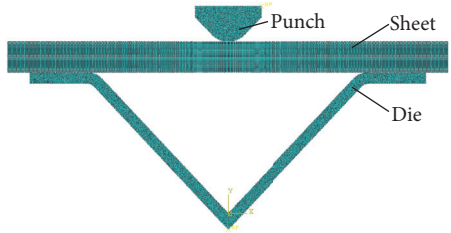

Figure 2: FE mesh model of bending process.

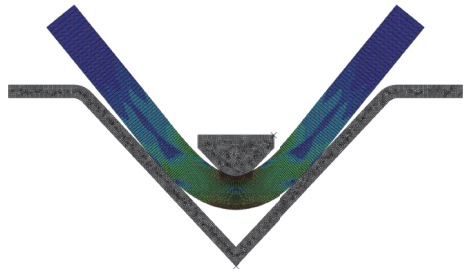

Figure 3: Second bending phenomenon of larger curved arc sheet.

3.4. Verification of FE Model. Aiming at validating the FE model, the FE simulated results are compared with the experiment under the same process conditions. There are many materials and process parameters in the FE model. The experimental verification on each FE model is unnecessary. Thus, a set of material and process parameters within the variable space is chosen randomly to implement the FE simulation and verification. Due to the randomness of selection, the real precision of FE model in Table 3 will be revealed.

Table 3: Experimental sample sets.

Number	t (mm)	R (mm)	r (mm)	M	$D_1 = 5$ mm α_1 (°)	$D_2 = 4.4$ mm α_2 (°)	$D_3 = 4$ mm α_3 (°)	$D_4 = 3$ mm α_4 (°)	$D_5 = 2.6$ mm α_5 (°)
1	1	0.2	0.2	0.61	88.11	96.72	101.39	118.34	125.54
2	1	0.6	0.6	1.15	83.47	92.97	99.77	118.44	126.47
3	1	0.6	0.6	1.85	90.73	99.77	106.07	122.52	129.9
4	1	1	1	1.93	93.67	101.96	107.87	124.54	131.66
5	1	1	1	2.07	88.77	99.68	105.74	122.74	130.19
6	1.4	0.2	0.6	1.85	86.81	97.11	102.98	120.13	127.86
7	1.4	0.6	0.6	1.93	91.68	99.86	105.84	122.73	130.14
8	1.4	0.6	1	2.07	84.92	96.65	102.9	120.46	127.96
9	1.4	1	1	0.61	85.93	95.04	101.35	118.91	126.5
10	1.4	1	0.2	1.15	79.22	90.8	97.89	116.89	125.43
11	1.4	0.2	0.6	2.07	84.79	96.41	102.02	119.42	127.2
12	1.4	0.6	1	0.61	86.03	94.57	100.69	118.1	125.52
13	1.4	0.6	1	1.15	78.1	89.59	96.67	115.74	124.02
14	1.4	1	0.2	1.85	91.04	99.4	105.52	122.62	129.96
15	1.4	1	0.6	1.93	92.05	100.31	106.35	123.4	130.73
16	2	0.2	1	1.15	73.48	85.85	92.78	113.22	121.76
17	2	0.6	1	1.85	83.6	94.41	101.03	119.38	127.46
18	2	0.6	0.2	1.93	90.36	98.98	105.25	122.8	130.36
19	2	1	0.6	2.07	84.13	95.18	101.94	120.19	128.12
20	2	1	0.6	0.61	83.8	93.02	99.68	118.07	126.2
21	2	0.2	1	1.93	84.79	95.21	101.68	119.98	127.83
22	2	0.6	0.2	2.07	85.72	96.08	102.54	120.54	128.27
23	2	0.6	0.6	0.61	83.5	92.63	99.17	117.55	125.35
24	2	1	0.6	1.15	77.06	88.29	95.12	115.18	124.03
25	2	1	1	1.85	83.76	94.66	101.62	120.16	128.11
T1	1.4	0.6	0.6	1.85	89.32	98.29	104.36	121.42	128.77
T2	2	0.2	0.2	1.93	90.11	98.68	104.89	122.32	129.77
T3	1.4	1	1	1.85	88.13	98.09	104.42	121.81	129.25
T4	1.4	1	0.6	2.07	86.4	97.6	103.87	121.41	128.9
T5	1	0.6	1	0.61	87.07	96.56	102.61	119.55	127.08

The sheet of steel material B340LA is selected randomly to carry out the experiment on the bending machine. D is directly observed from bending machine number control equipment named Delem. The sheet is unloaded directly after bending. It will undergo springback immediately. After springback, angle measurement instrument is used to measure the final bending angle α. α is the mean value of three bending angles which are measured from the same D. The experiment moulds are shown in Figure 4.

The experimental moulds and steel sheet parameters are as follows:

$$\begin{aligned} V &= 12\,\text{mm}, \\ \varphi &= 86^{\circ}, \\ R &= 1\,\text{mm}, \\ r &= 1\,\text{mm}, \\ t &= 1.4\,\text{mm}, \\ M &= 1.93. \end{aligned} \tag{2}$$

With the change of punch displacement, the comparisons of bending angles on FE simulation and experiment are shown in Figure 5.

In Figure 5, it can be found that the FE simulated bending angles are consistent with the bending experiment results. Most of bending angle deviations between FE and experiment are no more than 1 degree, and the largest bending angle deviation is only 1.63 degrees at the place where D = 3.177 mm. This indicates that the FE model has enough accuracy to simulate the bending springback process.

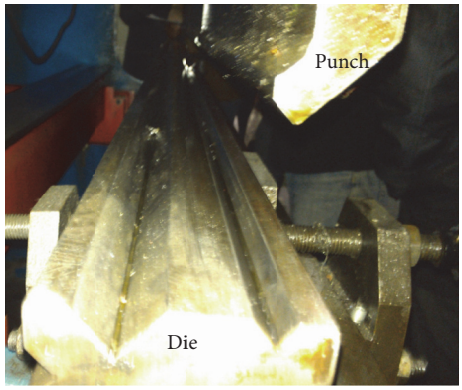

Figure 4: Moulds of bending experiment.

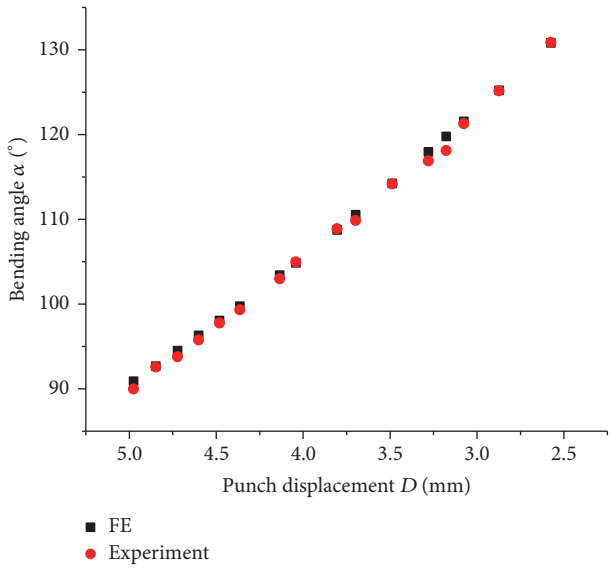

Figure 5: Comparison of bending angles on FE and experiment.

3.5. Effect of Length Ratio Factor on Bending Angle. As we all know, the geometrical position relationship of $V \neq 12$ mm is considered as a length ratio zooming on $V = 12$ mm. In this case, in terms of the bending process of $V \neq 12$ mm, its process parameters such as t, R, r, and D can be transformed by the length ratio zooming. Under this condition which transformed process parameters that belong to the range of Table 2, if the length ratio on the effect of bending angle is verified to be a small amount, the bending process of $V \neq 12$ mm is calculated by the BPNN-Spline model which is developed under the condition of $V = 12$ mm. This is beneficial to extend the application range of BPNN-Spline. The relationship between bending angle and length ratio factor ($\beta = V/12$) is discussed as follows.

A sample (the sample of number 3 is selected in this study) in Table 3 is randomly selected and its length values are zoomed by the ratio factors $\beta = 2$ and $\beta = 2.5$, respectively. It means that the nominal widths of die notch V are 24 mm and 30 mm, respectively. t, R, r, and D are also, respectively,

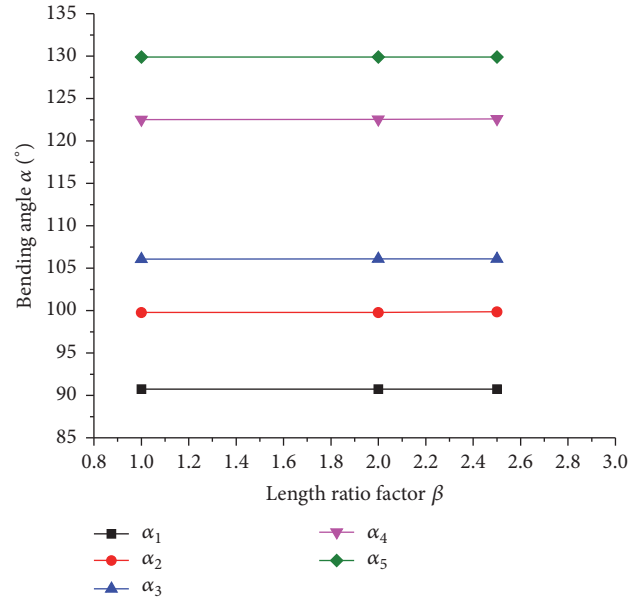

Figure 6: Effect of length ratio factor on bending angle.

zoomed by these length ratio factors. The effect of length ratio factor on bending angle is shown in Figure 6.

The effect of length ratio factor β on bending angle is so small that it is ignored. Therefore, the bending angle is unrelated with length ratio in the process.

4. Mathematical Model

4.1. Mathematical Model of BPNN. In this study, to develop the BPNN-Spline mathematical combination model, t, R, r, and M are treated as input parameters of BPNN, and D is treated as the input parameter of spline function.

The BPNN is trained and tested by the MATLAB software. Training is completed when the mean squared error (MSE) reached the minimum. The MSE formula is

$$\mathrm{MSE} = \frac{1}{n}\sum_{i=1}^{n}\left(\alpha_i - \widetilde{\alpha}_i\right)^2, \tag{3}$$

where n is the number of outputs, α_i is the ith predicted bending angle, and $\widetilde{\alpha}_i$ is the ith actual bending angle.

When α_i is directly treated as output of BPNN, the relationship between hidden layer node numbers and MSE of training and test are shown in Figure 7(a). Taking $\Delta\alpha_i = \alpha_i - A_i$ as the output of BPNN, the relationship between hidden layer node numbers and MSE of training and test are shown in Figure 7(b), where A_i are 85°, 95°, 100°, 120°, and 128°, respectively.

The training of BPNN in Figure 7(b) is better than Figure 7(a). When $\Delta\alpha_i$ is treated as output of BPNN, five output nodes will be set at the same magnitude level. This is more conducive to train the network. Thus, $\Delta\alpha_i$ is treated as the output of BPNN in this study. It can be seen that the BPNN will have a better comprehensive error for training and test when hidden layer node number is six, as shown in

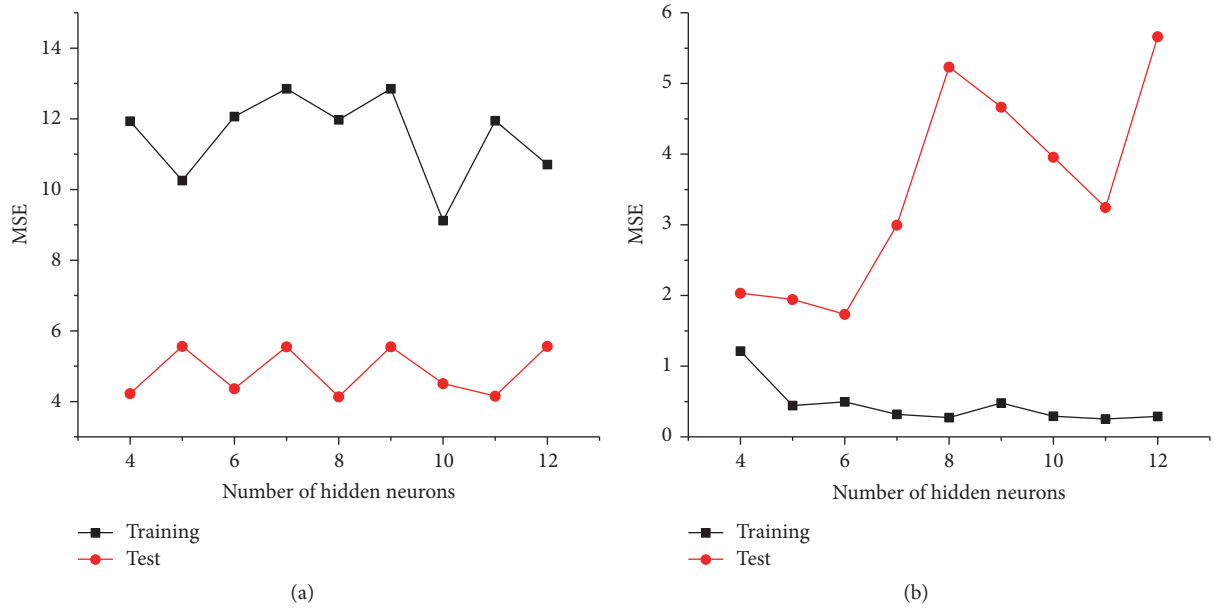

FIGURE 7: Effect of hidden layer node numbers on MSE for different output formats: (a) taking α_i as output; (b) taking $\Delta\alpha_i$ as the output.

Figure 7(b). As a result, the BPNN consisted of four input nodes, six hidden layer nodes, and five output nodes. The BPNN-Spline combined model is shown in Figure 8. The symmetrical sigmoid and purelin function are selected as the activation function on hidden and output layer, respectively. After the training and test, the MSE of training and test are 0.4947 and 1.7354, respectively.

A series of relation formulas between process parameters and bending angle can be obtained as follows:

$$\begin{aligned} \text{net}_j &= \sum_{i=1}^{n} \omega_{ij} x_i \\ f\left(\text{net}_j\right) &= \frac{1 - e^{-(\text{net}_j - b_j)}}{1 + e^{-(\text{net}_j - b_j)}} \\ \alpha_k &= \sum_{j=1}^{m} u_{jk} f\left(\text{net}_j\right) - B_k + A_k, \end{aligned} \tag{4}$$

where x_i, ω_{ij}, u_{jk}, b_j, and B_k are the input, connection weight between input and hidden layer, connection weight between hidden layer and output, and threshold values of hidden and output layer, respectively.

The BPNN model could be considered as a black box function which is the mapping between bending process parameters and bending angles:

$$\alpha_k = \text{BPNN}\left(t, R, r, M\right). \tag{5}$$

4.2. Combined Model of BPNN-Spline. Five α_k as the outputs of BPNN are, respectively, corresponding to D_i in Table 3; this one-to-one corresponding relation is equivalent to five points such as (D_1, α_1), (D_2, α_2), (D_3, α_3), (D_4, α_4), and (D_5, α_5). The five points are treated as interpolation points; a cubic spline function will be fitted, as shown in Figure 9 and (6). D and α are, respectively, treated as the independent variable and dependent variable.

$$\alpha = \text{Spline}\left(D\right). \tag{6}$$

The combination of (5) and (6) derives the following:

$$\alpha = \text{BPNN} - \text{Spline}\left(t, R, r, M, D\right). \tag{7}$$

Equation (7) is obtained on the precondition of $V = 12$ mm. Because the length ratio factor was defined as $\beta = V/12$, when the bending process parameters are t_1, R_1, r_1, and D_1, the bending angle is predictable based on the conversion of process parameters as the formula t_1/β, R_1/β, r_1/β, and D_1/β. Treating β as an input parameter, (7) can be written as

$$\alpha = \text{BPNN} - \text{Spline}\left(t, R, r, M, D, \beta\right). \tag{8}$$

Equation (8) is a general prediction model on bending springback process.

4.3. Comparison with Traditional BPNN. In order to verify the advantage of BPNN-Spline, its prediction accuracy is compared with traditional BPNN based on the FE simulation results of Section 3.4, as shown in Figure 10.

Traditional BPNN is a network by taking α as the output, t, R, r, M, and D as the inputs, and eight as the number of hidden layer nodes. The anterior 25 samples in Table 3 are normalized to train the BPNN (where α is the unique output, the training sample number becomes 125). The MSE of training and test are 11.2 and 6.8, respectively.

In Figure 10, the bending angle deviation between traditional BPNN and FE is larger. The biggest deviation is 6.5 degrees, which does not meet the accuracy requirement.

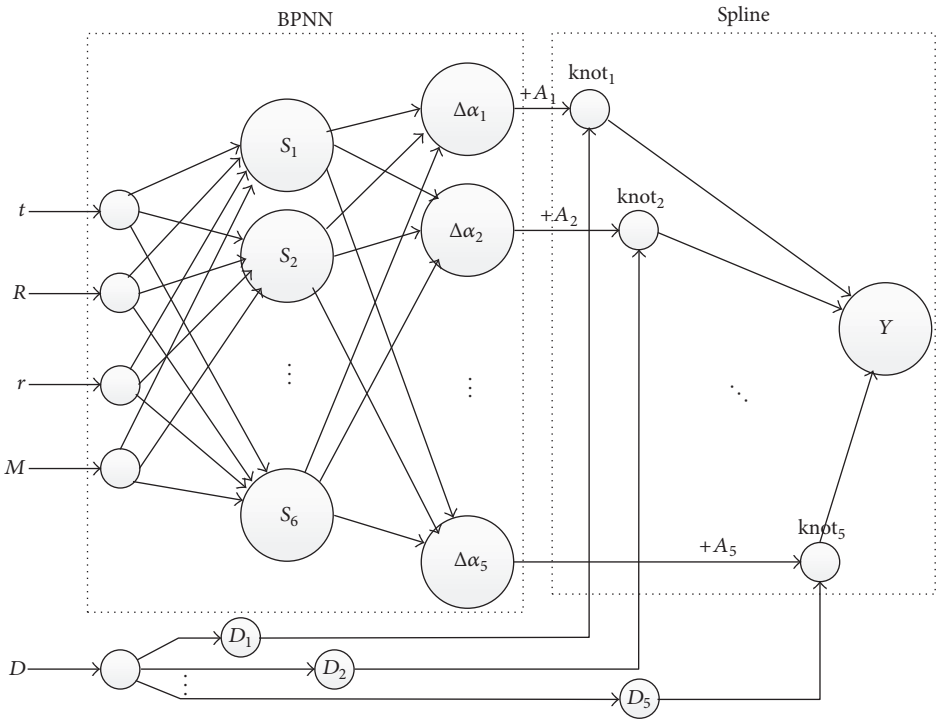

Figure 8: Diagram of BPNN-Spline combined model.

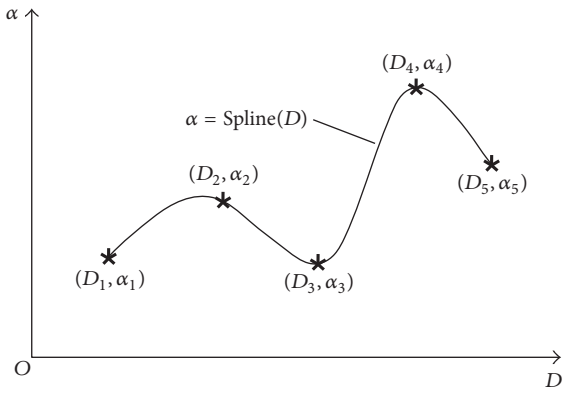

Figure 9: Fitted spline curve diagram.

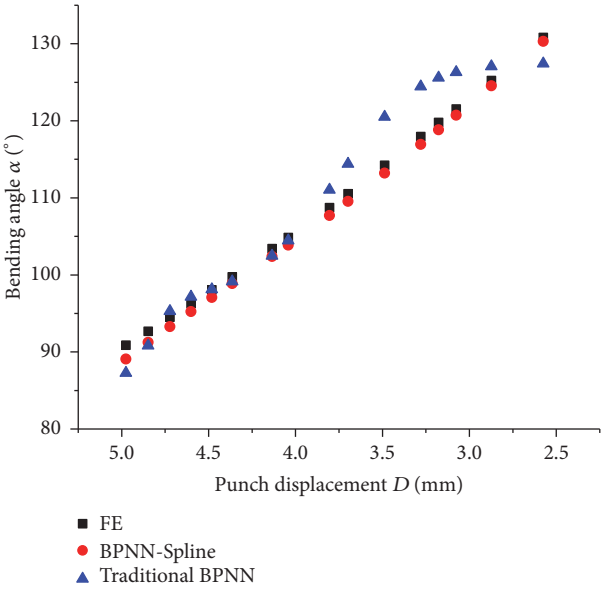

Figure 10: Comparison of prediction accuracy between BPNN-Spline and traditional BPNN.

However, the bending angle deviation between BPNN-Spline and FE is so small that the biggest deviation is only 1.78 degrees. Thus, BPNN-Spline is more precise in comparison with the traditional BPNN method.

4.4. Discussion. To predict the bending angle, the BPNN-Spline has great advantages in comparison with the traditional BPNN model. It mainly displays two aspects: The higher training accuracy and monotonic decrease relationship between α and D are easier to ensure. The explanation is as follows.

The bending angle α is related to t, R, r, M, and D. When building a traditional BPNN to predict the bending angle, t, R, r, M, and D need to be set as the input parameters, and α needs to be set as the unique output parameter. α is roughly distributed from 90 to 130 degrees, and this large range requires the traditional BPNN to have enough precision. A precise training of the traditional BPNN is very difficult to achieve. However, the BPNN in BPNN-Spline can be easily

trained to a precise degree in comparison with the traditional BPNN. When the BPNN in the BPNN-Spline is built, t, R, r, and M are set as inputs, and five bending angles α_i corresponding to each certain punch displacement D_i are set as outputs, respectively. Four variable inputs of the BPNN in BPNN-Spline are fewer, and the range of bending angle α_i is also smaller.

As far as we know, the monotonic decrease relationship between α and D is inevitable in bending process when other parameters are determined. This monotonic relationship is very important for prediction accuracy. Due to the characteristics of network structure, traditional BPNN is not able to ensure the monotonic relationship between α and D. But the smooth spline function in BPNN-Spline is easier to ensure this monotonic relationship in comparison with the traditional BPNN, as shown in Figure 10. As a consequence, the spline function in BPNN-Spline is more likely to obtain the accurate prediction results in bending process.

5. Application Examples and Discussion

The BPNN-Spline model is suitable for bending angle prediction in the case:

(a) If $\varphi = 86^\circ$ and $V = 12$ mm, the applicable variable space is $1\text{ mm} < t < 2\text{ mm}$, $0.2\text{ mm} < R < 1\text{ mm}$, $0.2\text{ mm} < r < 1\text{ mm}$, and $2.6\text{ mm} < D < 5\text{ mm}$.

(b) If $\varphi = 86^\circ$ and $V \neq 12$ mm, the length ratio factor is $\beta = V/12$. The applicable variable space is $\beta\text{ mm} < t < 2\beta\text{ mm}$, $0.2\beta\text{ mm} < R < \beta\text{ mm}$, $0.2\beta\text{ mm} < r < \beta\text{ mm}$, and $2.6\beta\text{ mm} < D < 5\beta\text{ mm}$.

Six application examples under diverse material, process parameter, and length ratio factor are randomly selected to determine the prediction accuracy of BPNN-Spline. The predicted bending angles are compared with FE simulation results, as shown in Figures 11(a), 11(b), 11(c), 11(d), 11(e), and 11(f).

In Figure 11, it can be observed that the predicted bending angle of BPNN-Spline is in good agreement with FE simulation results for diverse material, nominal width of die notch, die corner radius, punch corner radius, sheet thickness, and punch displacement. The bending angle deviations between BPNN-Spline and FE are so small that the biggest one is no more than 1.2 degrees, which is at the place where $D = 4.7$ mm in Figure 11(c). Therefore, it can be concluded that the BPNN-Spline model has enough accuracy to predict the bending angle under diverse bending condition.

In order to determine the prediction accuracy of BPNN-Spline in actual bending experiment aspect, two kinds of sheet are randomly selected to carry out the bending experiment. The results are compared with BPNN-Spline predicted results under the same process conditions. The sheets of steel material B340LA with 1.4 mm thickness and DP600 with 1.8 mm thickness are, respectively, used to carry out the experiment on the bending machine. The experimental mould and other process parameters are the same as the experiments of Section 3.4.

The comparisons between experiential and BPNN-Spline predicted bending angles are shown in Figures 12(a) and 12(b), respectively.

As can be seen from Figure 12, predicted bending angles by BPNN-Spline are consistent with the experiment results. The largest bending angle deviation between BPNN-Spline and experiment for B340LA is no more than 1.4 degrees, which is at the place where $D = 4.8$ mm. The largest bending angle deviation for DP600 is no more than 1 degree, which is at the place where $D = 2.95$ mm. The prediction precision of BPNN-Spline is verified by actual bending experiments. In conclusion, the BPNN-Spline model can accurately predict the bending angle in actual production process. The technical requirement on BPNN-Spline model is lower compared to FE simulation. The user only needs to take the model as a black box and input the material and bending process parameters into the model; the corresponding bending angle will be deduced out immediately. It is very convenient and efficient.

The bending machine numerical control system should accurately and rapidly deduce out the bending angle for diverse process parameters. Therefore, BPNN-Spline combined model could be integrated properly into the system to control the bending process.

6. Conclusions

A bending springback angle prediction model based on the combination of BPNN and spline is presented in this study. Firstly, through FE and orthogonal experimental design, the training sample set is obtained. After that, the mathematical model of BPNN-Spline is established, and its advantage for bending angle prediction is discussed in comparison with traditional BPNN. Finally, through application examples, the BPNN-Spline model is used to predict the bending angle and shows higher prediction accuracy. The following conclusions are summarized:

(1) The bending angle is unrelated with length ratio factor β.

(2) BPNN-Spline combined model is better than traditional BPNN on bending angle prediction. This is because the BPNN-Spline combined model has special network structure and smooth spline function, which will bring about a great advantage for the bending angle prediction.

(3) The BPNN-Spline combined model shows better prediction accuracy on different material, thickness, nominal width of die notch, and other process parameters by the test of application examples; the general and precise characteristics are fully revealed.

(4) The BPNN-Spline combined model not only has better applicable ability, but also has higher prediction accuracy.

Although the BPNN-Spline model has a good performance under the case of $\varphi = 86^\circ$, it still cannot be applied in the case of $\varphi < 86^\circ$. Future study should develop a model which can predict the bending angle accurately with respect to the case of $\varphi < 86^\circ$.

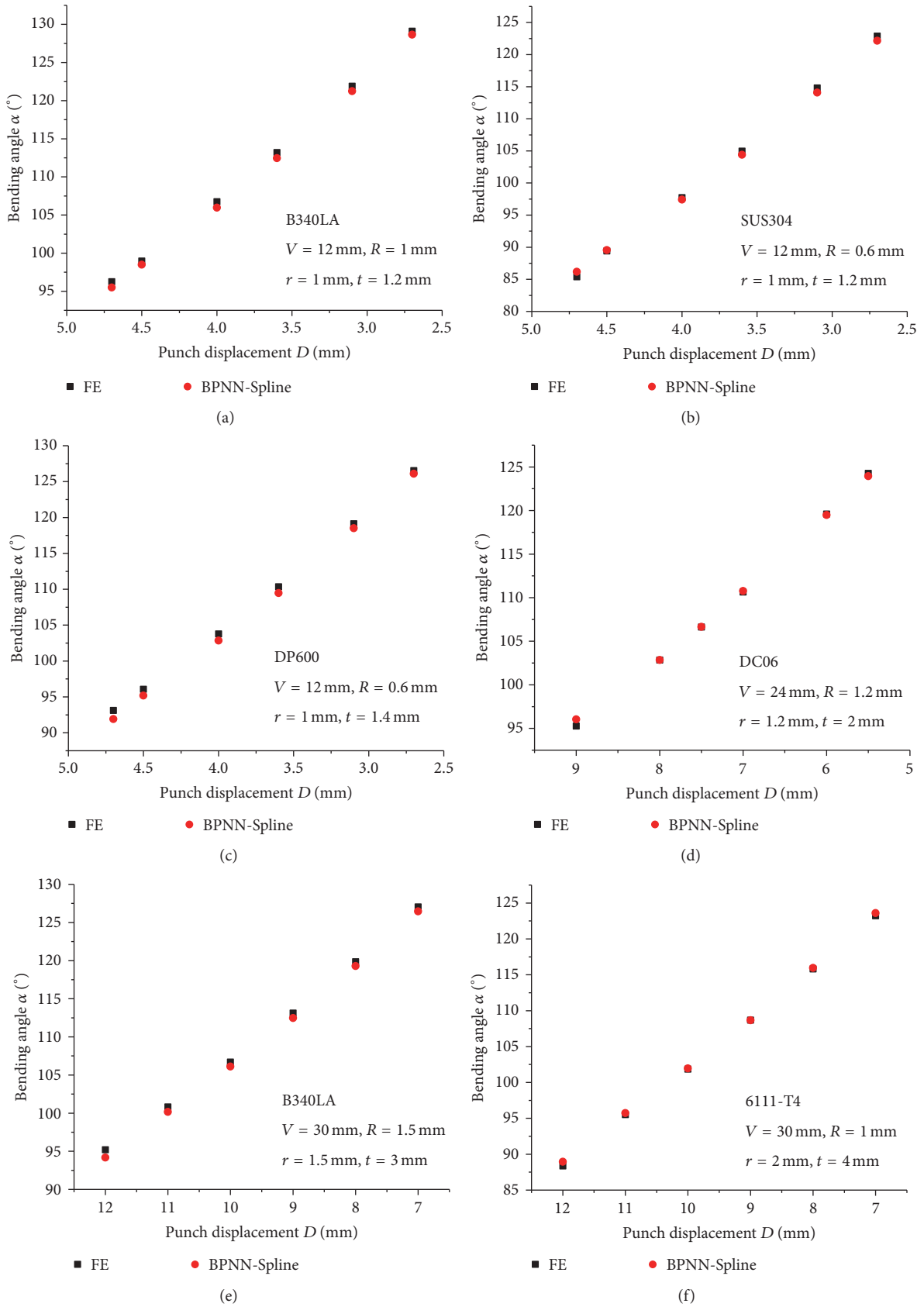

Figure 11: Comparison of FE and BPNN-Spline: (a) B340LA with $t = 1.2$ mm, $V = 12$ mm, $R = 1$ mm, $r = 1$ mm; (b) SUS304 with $t = 1.2$ mm, $V = 12$ mm, $R = 0.6$ mm, $r = 1$ mm; (c) DP600 with $t = 1.4$ mm, $V = 12$ mm, $R = 0.6$ mm, $r = 1$ mm; (d) DC06 with $t = 2$ mm, $V = 24$ mm, $R = 1.2$ mm, $r = 1.2$ mm; (e) B340LA with $t = 3$ mm, $V = 30$ mm, $R = 1.5$ mm, $r = 1.5$ mm; and (f) 6111-T4 with $t = 4$ mm, $V = 30$ mm, $R = 1$ mm, $r = 2$ mm.

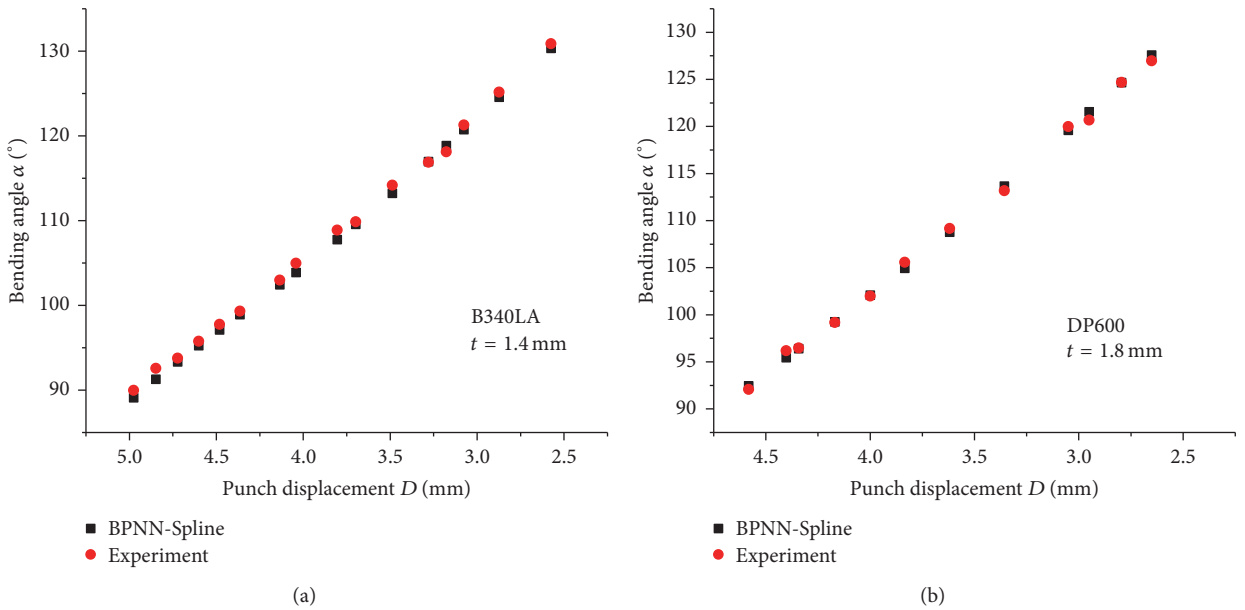

Figure 12: Comparison of BPNN-Spline and experiment: (a) B340LA with 1.4 mm thickness; (b) DP600 with 1.8 mm thickness.

Competing Interests

The authors declare that they have no competing interests.

Acknowledgments

The research is continuously funded by the National Science and Technology Major Project of China (2012ZX0401031).

References

[1] D.-K. Leu, "Position deviation and springback in V-die bending process with asymmetric dies," *International Journal of Advanced Manufacturing Technology*, vol. 79, no. 5–8, pp. 1095–1108, 2015.

[2] S. V. Mohammadi, M. Parsa, and M. Parsa, "Simplified springback prediction in Al/PP/Al sandwich air bending," *Journal of Sandwich Structures and Materials*, vol. 17, no. 3, pp. 217–237, 2015.

[3] L. J. De Vin, "Expecting the unexpected, a must for accurate brakeforming," *Journal of Materials Processing Technology*, vol. 117, no. 1-2, pp. 244–248, 2001.

[4] Y. Zong, P. Liu, B. Guo, and D. Shan, "Springback evaluation in hot v-bending of Ti-6Al-4V alloy sheets," *International Journal of Advanced Manufacturing Technology*, vol. 76, no. 1–4, pp. 577–585, 2015.

[5] V. Vorkov, R. Aerens, D. Vandepitte, and J. R. Duflou, "Springback prediction of high-strength steels in large radius air bending using finite element modeling approach," in *Proceedings of the 11th International Conference on Technology of Plasticity (ICTP '14)*, pp. 1005–1010, Nagoya, Japan, October 2014.

[6] Z. M. Fu, W. Chen, X. L. Tian, and B. K. Hu, "Modeling and simulation for multiple-step incremental air-bending forming of sheet metal," *International Journal of Advanced Manufacturing Technology*, vol. 72, no. 5–8, pp. 561–570, 2014.

[7] M. R. Jamli, A. K. Ariffin, and D. A. Wahab, "Incorporating feedforward neural network within finite element analysis for L-bending springback prediction," *Expert Systems with Applications*, vol. 42, no. 5, pp. 2604–2614, 2015.

[8] M. Haddadzadeh, M. R. Razfar, and M. R. M. Mamaghani, "Novel approach to initial blank design in deep drawing using artificial neural network," *Proceedings of the Institution of Mechanical Engineers, Part B: Journal of Engineering Manufacture*, vol. 223, no. 10, pp. 1323–1330, 2009.

[9] H. Hasanzadehshooiili, A. Lakirouhani, and A. Šapalas, "Neural network prediction of buckling load of steel arch-shells," *Archives of Civil and Mechanical Engineering*, vol. 12, no. 4, pp. 477–484, 2012.

[10] K. Hiramoto, "Control system design of mechanical systems with time varying mechanical and control parameters," *Journal of Advanced Mechanical Design, Systems, and Manufacturing*, vol. 8, no. 3, pp. 1–14, 2014.

[11] J. Xu, K. Yamada, K. Seikiya, R. Tanaka, and Y. Yamane, "Comparison of applying static and dynamic features for drill wear prediction," *Journal of Advanced Mechanical Design, Systems and Manufacturing*, vol. 8, no. 4, p. JAMDSM0056, 2014.

[12] S. Kitayama, S. Huang, and K. Yamazaki, "Optimization of variable blank holder force trajectory for springback reduction via sequential approximate optimization with radial basis function network," *Structural and Multidisciplinary Optimization*, vol. 47, no. 2, pp. 289–300, 2013.

[13] J. Srirat, S. Kitayama, and K. Yamazaki, "Simultaneous optimization of variable blank holder force trajectory and tools motion in deep drawing via sequential approximate optimization," *Journal of Advanced Mechanical Design, Systems and Manufacturing*, vol. 6, no. 7, pp. 1081–1092, 2012.

[14] J.-H. Song, H. Huh, and S.-H. Kim, "Stress-based springback reduction of a channel shaped auto-body part with high-strength steel using response surface methodology," *Journal of Engineering Materials and Technology, Transactions of the ASME*, vol. 129, no. 3, pp. 397–406, 2007.

[15] X.-Y. Guo, D. Li, Z. Wu, and Q.-H. Tian, "Application of response surface methodology in optimizaing the sulfation-roasting-leaching process of nickel laterite," *International Journal of Minerals, Metallurgy and Materials*, vol. 19, no. 3, pp. 199–204, 2012.

[16] C. Shen, L. Wang, and Q. Li, "Optimization of injection molding process parameters using combination of artificial neural network and genetic algorithm method," *Journal of Materials Processing Technology*, vol. 183, no. 2-3, pp. 412–418, 2007.

[17] Y. Rostamiyan, A. Seidanloo, H. Sohrabpoor, and R. Teimouri, "Experimental studies on ultrasonically assisted friction stir spot welding of AA6061," *Archives of Civil and Mechanical Engineering*, vol. 15, no. 2, pp. 335–346, 2015.

[18] M. Winnicki, A. Małachowska, and A. Ambroziak, "Taguchi optimization of the thickness of a coating deposited by LPCS," *Archives of Civil and Mechanical Engineering*, vol. 14, no. 4, pp. 561–568, 2014.

[19] Y. Tzeng, F. Chen, and C. Chen, "A hybrid approach for multi-objective design optimization of ball grid array gold wire bonding process," *Journal of Advanced Mechanical Design, Systems, and Manufacturing*, vol. 9, no. 2, p. JAMDSM0021, 2015.

[20] M. Piffl and E. Stadlober, "The depth-design: an efficient generation of high dimensional computer experiments," *Journal of Statistical Planning and Inference*, vol. 164, pp. 10–26, 2015.